

PAPER

Compact and Athermal DQPSK Demodulator with Silica-Based Planar Lightwave Circuit

Yusuke NASU^{†a)}, Yohei SAKAMAKI[†], Kuninori HATTORI[†], Shin KAMEI[†], Toshikazu HASHIMOTO[†], Takashi SAIDA[†], *Members*, Hiroshi TAKAHASHI[†], and Yasuyuki INOUE[†], *Senior Members*

SUMMARY We present a full description of a polarization-independent athermal differential quadrature phase shift keying (DQPSK) demodulator that employs silica-based planar lightwave circuit (PLC) technology. Silica-based PLC DQPSK demodulator has good characteristics including low polarization dependence, mass producibility, etc. However delay line interferometer (DLI) of demodulator had the large temperature dependence of its optical characteristics, so it required large power consumption to stabilize the chip temperature by the thermo-electric cooler (TEC). We previously made a quick report about an athermal DLI to reduce a power consumption by removing the TEC. In this paper, we focus on the details of the design and the fabrication method we used to achieve the athermal characteristics, and we describe the thermal stability of the signal demodulation and the reliability of our demodulator. We described two athermalization methods; the athermalization of the transmission spectrum and the athermalization of the polarization property. These methods were successfully demonstrated with keeping a high extinction ratio and a small footprint by introducing a novel interwoven DLI configuration. This configuration can also limit the degradation of the polarization dependent phase shift (PDF) to less than 1/10 that with the conventional configuration when the phase shifters on the waveguide are driven. We used our demodulator and examined its demodulation performance for a 43 Gbit/s DQPSK signal. We also verified its long-term reliability and thermal stability against the rapid temperature change. As a result, we confirmed that our athermal demodulator performed sufficiently well for use in DQPSK systems.

key words: differential quadrature phase-shift keying (DQPSK), Mach-Zehnder, Delay-line interferometer, optical planar waveguides

1. Introduction

Return-to-zero differential quadrature phase-shift keying (RZ-DQPSK) is considered a leading candidate for 40 Gbit/s transmission systems as a result of its high spectral efficiency, high receiver sensitivity and large tolerance to impairment factors such as chromatic dispersion, polarization mode dispersion and bandwidth narrowing at optical add drop multiplexers [3], [4]. In comparison with conventional on-off keying, however, the RZ-DQPSK format requires more complicated transmitters and receivers for modulating and demodulating RZ-DQPSK format signals, respectively. To provide “green” and cost effective transmission systems, it is becoming increasingly important to reduce both the footprint and power consumption of the transmitters and receivers.

One of the key components on the receiver side is a de-

modulator, which generally consists of two delay-line interferometers (DLIs) with a 90° phase offset. Various types of DQPSK demodulators have been proposed, including those based on free space optics [5], optical fiber [6], and planar lightwave circuits (PLCs) [7]–[9]. Of these, the silica-based PLC demodulator [8], [9] has a number of advantages over the other configurations including high speed tuning characteristics, good mass producibility, high reliability, low polarization dependence and the potential for full integration with balanced receivers.

The first-generation silica-based PLC demodulator has already been deployed in the field. However, its power consumption is relatively large, because it is equipped with a thermo-electric cooler (TEC) to stabilize the chip temperature. The TEC accounts for about 70% of the total power consumption.

Recently, we proposed the athermal DQPSK demodulator, and achieved a 60% reduction in the power consumption by removing the TEC [1], [2]. In this paper, we focus on the detail design to achieve such athermal condition of the DLI with keeping low polarization dependence, high extinction ratio and low loss. In addition, we also report the additional investigation on thermal stability and reliability of our DQPSK demodulator.

In Sect. 2, we discuss the design of the athermal DQPSK demodulator. There are two issues related to demodulator athermalization. The first involves finding a way to athermalize the transmission spectrum of the demodulator. Since the refractive index of silica glass depends on the PLC chip temperature, the DLI transmission spectrum shifts by 1.4 GHz/°C. We use resin filled grooves to compensate for the temperature dependence of the silica, which is similar to the technique used for athermal arrayed-waveguide gratings (AWGs) [21]. We discuss the groove design in detail in Sect. 2.1. It should be noted that, when designing an athermal DQPSK demodulator, we must take account of both the excess loss and the loss imbalance at the grooves, if we are to achieve a good extinction ratio.

The second issue with respect to athermalization involves finding a way to athermalize the birefringence of the waveguide. To improve the polarization dependent frequency shift (PDF), which is one of the key parameters of the DQPSK demodulator [12], [13], it is important to set the birefringence at a specific value [10], [15]–[19]. Thus, it is important to eliminate the temperature dependence of the birefringence. In Sect. 2.2, we discuss the temperature de-

Manuscript received February 3, 2010.

Manuscript revised March 27, 2010.

[†]The authors are with NTT Photonics Laboratories, NTT Corporation, Atsugi-shi, 243-0198 Japan.

a) E-mail: nasu@aecl.ntt.co.jp

DOI: 10.1587/transele.E93.C.1191

pendence of the birefringence in detail.

In Sect. 3, we report the fabrication of the athermal demodulators. We have applied the athermalization technologies discussed in Sect. 2 to a DQPSK demodulator with an interwoven configuration [21]. The interwoven configuration enables us to halve the conventional chip size. Moreover, it allows us to eliminate the PDF increase caused by the birefringence change when the phase shifter is driven. We describe the design of the interwoven configuration in Sect. 3.1. Finally, in Sect. 3.2, we discuss the performance of the fabricated DQPSK demodulator, and report bit error rate (BER) measurement, demodulation stability against the rapid temperature change, and reliability test results.

2. Athermalization of Delay-Line Interferometer

2.1 Athermalization of Transmission Spectrum

In this section, we describe the athermalization of a silica-based DLI. In this Sect. 2.1, we describe the athermalization of the transmission spectrum, and in next subsection, we describe the athermalization of the polarization property of the DLI.

The transmission peak of a silica-based demodulator has a temperature dependence of $1.4 \text{ GHz}/^\circ\text{C}$, due to the temperature dependent refractive index of silica. This temperature dependence can be compensated by filling grooves in the DLI with resin that has a negative temperature dependence. Although this technique is similar to that used for athermal AWGs [21], we need to optimize the groove design to apply it to the DQPSK demodulator.

Figure 1 is a schematic of a DLI with resin-filled grooves. We used multiply divided grooves to reduce the diffraction loss at the grooves. Grooves are formed in both arms of the DLI to prevent any extinction ratio degradation induced by an excess loss imbalance between the arms. The difference between the total groove lengths of the arms is set to compensate for the temperature dependent refractive index of the silica waveguide. It should be noted that this

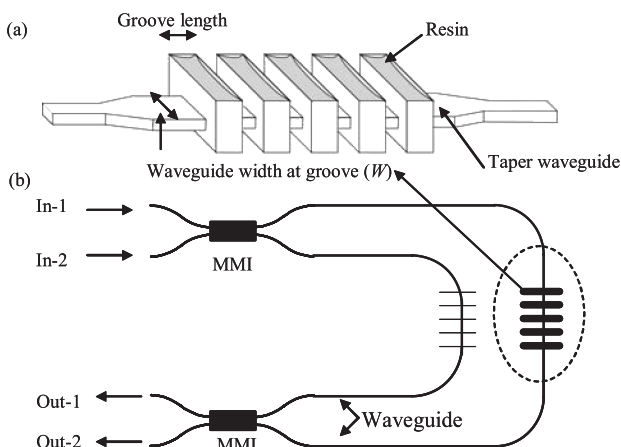


Fig. 1 Schematic figure of the resin-filled groove across the waveguide (a) and the single Delay-line interferometer.

configuration is tolerant to groove length fluctuations resulting from the etching process as both arms are equipped with the same number of grooves.

First, we optimized the total groove length difference experimentally. We fabricated the DLI using silica-based PLC technologies. The refractive index difference and waveguide core thickness were 1.5% and $4.5 \mu\text{m}$, respectively. The cladding and core were deposited on a Si substrate by flame hydrolysis deposition, and the waveguide was formed by photolithography and etching. The free spectral range (FSR) of the DLI was set at 21.9 GHz , which is a value widely used for 43 Gbit/s DQPSK demodulation.

Figure 2 shows the measured maximum spectral shift of our fabricated DLI over a temperature range of -10 to 70°C as a function of total groove length difference. The spectral shift was the smallest at a total groove length difference of $261 \mu\text{m}$. This length agrees with the value calculated from the temperature dependence of the refractive indexes of silica glass ($1 \times 10^{-5}/^\circ\text{C}$) and the resin material ($-37 \times 10^{-5}/^\circ\text{C}$). The slight residual spectral shift of 8.8 GHz was due to the second-order components of the temperature dependence of silica glass, and this was sufficiently small to be compensated with phase shifters.

Next, we optimized the number of grooves. Here it is important to reduce the loss imbalance between the arms as well as the excess loss at each arm, because the loss imbalance degrades the extinction ratio of the DLI.

Figures 3(a) and (b) show the measured excess loss and the excess loss imbalance of the arm, respectively, when we changed the waveguide width at the grooves and the number of grooves. The groove interval was $30 \mu\text{m}$. As seen in Fig. 3(a), although a wider waveguide generally has a better excess loss, the excess loss depends strongly on the waveguide width and groove number. This is because the divided grooves function as a weak long-period grating [22]. As for the excess loss imbalance, a waveguide width of $12 \mu\text{m}$ provides the best result. The behaviors of the excess loss and excess loss imbalance were complicated, so we tried to find the optimum value of the groove number and waveguide width experimentally. Finally we set them as 20 and $12 \mu\text{m}$, respectively.

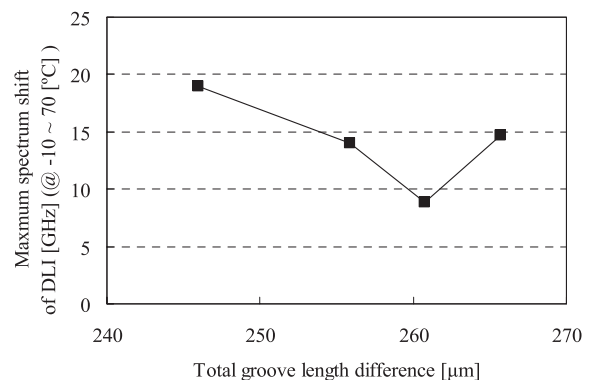


Fig. 2 Maximum spectrum shift of fabricated DLI as a function of total groove length difference.

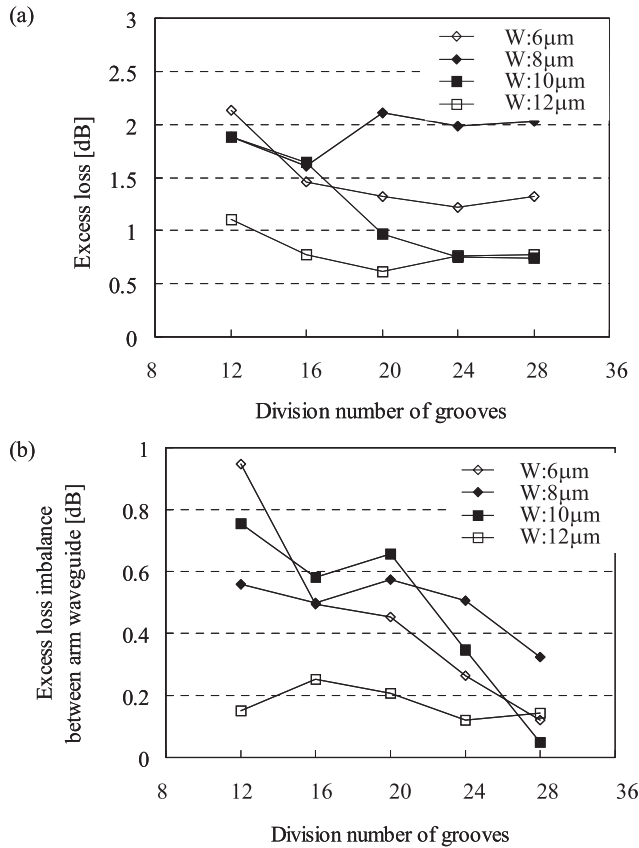


Fig. 3 (a) Excess loss and (b) excess loss imbalance at the grooves as a function of waveguide width (W) and number of grooves.

To evaluate the impact of an excess loss imbalance of 0.2 dB, we calculated the extinction ratio of the DLI by using 2by2 transmission matrix. The calculation took account of the loss imbalance at the couplers. We used 2×2 multimode interference (MMI) couplers as the divider and combiner in the DLI. In general, an MMI coupler optimized for the smallest excess loss is not always optimized for the smallest loss imbalance [24]. The MMI coupler that we used in our DLI had a loss imbalance of 0.35 dB between two outputs. Figure 4 shows the calculated extinction ratio dependence on the loss imbalance at the waveguide arms. As shown in the figure, the extinction ratio from port In-1 is better than that from port In-2. This is because the excess loss imbalance at the waveguide arms is canceled out by the loss imbalance at the couplers when port In-1 is used.

Figure 5 shows the measured extinction ratio of our DLI, which agrees with our calculation results. We confirmed experimentally that by using input port In-1 an extinction ratio of about -30 dB can be achieved over a wide wavelength range of 1520 to 1620 nm.

Finally, we measured the DLI fabricated with the optimized groove parameters. Figure 6 shows the measured temperature dependent center frequency shift of the DLI. The frequency shift within a -20 to 70°C temperature range was suppressed to less than 1/10 that of a conventional DLI.

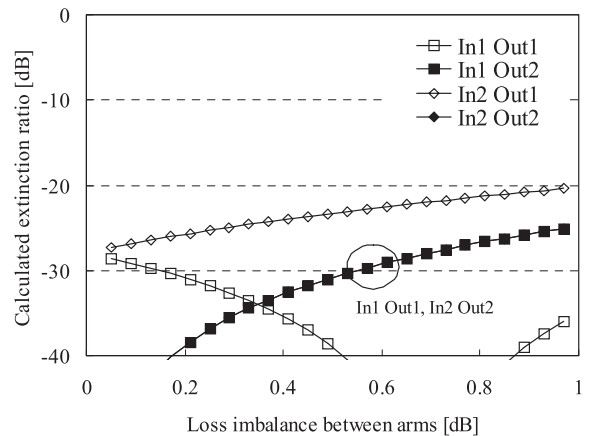


Fig. 4 Calculated extinction ratio of DLI. The loss imbalance is the excess loss difference between waveguide arms with resin-filled grooves. This is positive when the excess loss of the long arm is larger than that of the short arm. The port number in the legend is defined in Fig. 1(b). The MMI coupling ratio was 0.48.

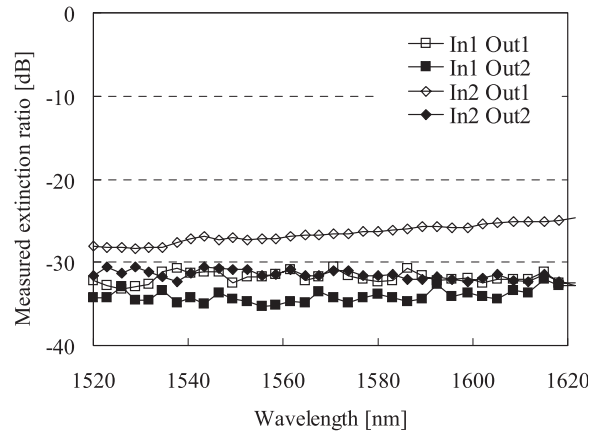


Fig. 5 Measured extinction ratio of DLI.

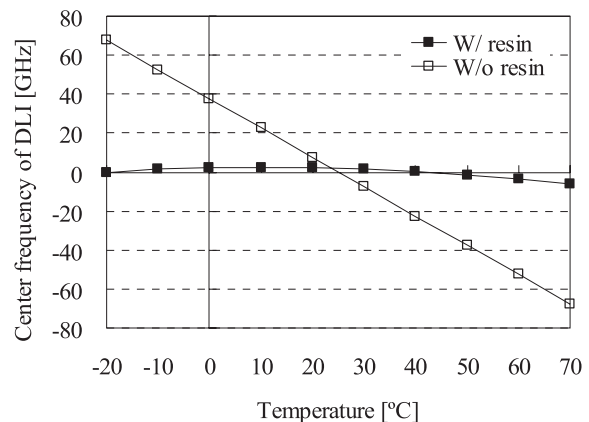


Fig. 6 Spectral shift of DLI with changing temperature.

The remaining frequency shift was sufficiently small to be eliminated by the phase shifter on the DLI.

2.2 Athermalization of Birefringence

Polarization dependence, one of the key parameters of a DQPSK demodulator, depends strongly on the waveguide birefringence. In terms of polarization dependence, the PDF in particular is changed when the birefringence changes with temperature. Therefore, to realize an athermal DQPSK demodulator, we need to eliminate the temperature dependence of the birefringence as well as the temperature dependence of the refractive index.

The birefringence of our conventional PLC has a temperature dependence of $1.0 \times 10^{-5}/^\circ\text{C}$. This change is negligible for conventional PLC applications such as AWGs and optical switches. However, it must be suppressed for DQPSK demodulator applications.

Birefringence generally results from asymmetric stress around a waveguide core. The birefringence, B , is written with the horizontal (σ_x) and vertical (σ_y) components of the stress in the core (horizontal means it is horizontal to the Si substrate) as

$$B = C \cdot (\sigma_x - \sigma_y), \quad (1)$$

where C is the stress optic coefficient. The asymmetric stress in the core, $\sigma_x - \sigma_y$, develops during high-temperature processes such as glass deposition. Although the amount of stress is determined by the thermal expansion coefficients of each layer (Si substrate, cladding and core) and its thermal history, we can use the approximation that the stress results from the overcladding deposition [25]. In this case, the asymmetric stress can be represented by the difference between the thermal expansion coefficients of the silicon substrate (α_{Si}) and that of the overcladding glass (α_{OC}) as

$$\sigma_x - \sigma_y \approx \sigma_x = \int_T^{T_g} \frac{E_{OC}(\alpha_{Si} - \alpha_{OC})}{1 - \nu_{OC}} dT. \quad (2)$$

E_{OC} and ν_{OC} are Poisson's ratio and Young's modulus of the overcladding glass, respectively. T is the temperature,

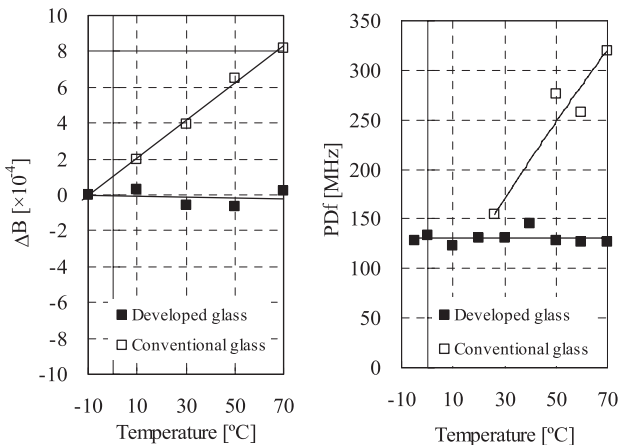


Fig. 7 Temperature dependence of birefringence (a) and PDF (b) with conventional glass and developed glass.

and T_g is the temperature at which the overcladding glass begins to generate stress. We thus obtain the temperature dependence of waveguide birefringence as

$$\frac{dB}{dT} \approx \frac{C \cdot E_{OC}(\alpha_{Si} - \alpha_{OC})}{1 - \nu_{OC}}. \quad (3)$$

As shown in Eq. (3), we can eliminate the temperature dependence of the waveguide birefringence by matching the thermal expansion coefficient of the glass (α_{OC}) to that of the silicon substrate (α_{Si}). The thermal expansion coefficient of the glass can be engineered by controlling its dopant concentration [25].

We fabricated DLI circuits to confirm that the temperature dependence of the waveguide birefringence was suppressed. We used two types of overcladding glass; one was conventional glass and the other was the glass we developed to suppress the temperature dependence of the birefringence. Figure 7(a) shows the measured temperature dependent birefringence, where we estimated the birefringence from the spectral shift between the transverse electric (TE) and transverse magnetic (TM) modes. We confirmed that the temperature dependence of the birefringence was successfully suppressed over a wide temperature range.

Figure 7(b) shows the measured PDF as a function of DLI temperature, where the PDF was estimated from the measured Mueller matrix of the DLI. We successfully reduced the temperature dependence of the PDF with the developed glass to less than 1/10 of that with conventional glass.

3. Evaluation of Athermal DQPSK Demodulator

3.1 Interwoven Layout of Athermal DQPSK Demodulator

Basically, a DQPSK demodulator is equipped with two DLIs. Both DLIs have a time delay of approximately one symbol period, and a phase difference of 90° . Figure 8 shows the circuit layout of a DQPSK demodulator based on our proposed interwoven DLI configuration [20]. The two DLIs are interwoven to reduce their footprint. A half-wave plate is installed between the DLIs to compensate for their polarization dependence. The thin film heaters used to tune the center frequency of the DLIs and the resin filled

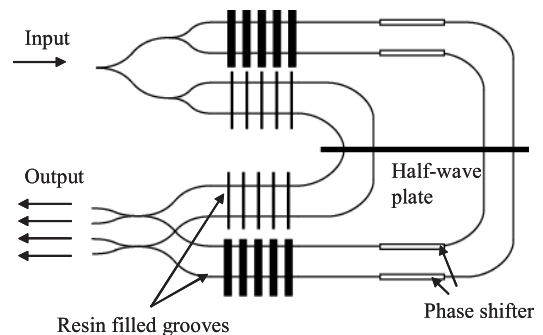


Fig. 8 Circuit of DQPSK demodulator with interwoven configuration.

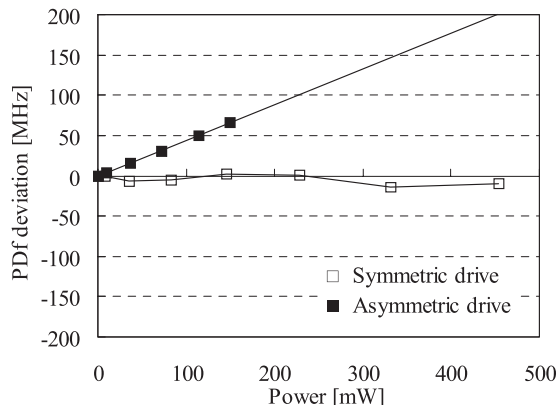


Fig. 9 The PDF change when the phase shifter is driven. “Symmetric” means the same power is applied to the heaters on both sides of the half-wave plate. “Asymmetric” means the power is applied unilaterally.

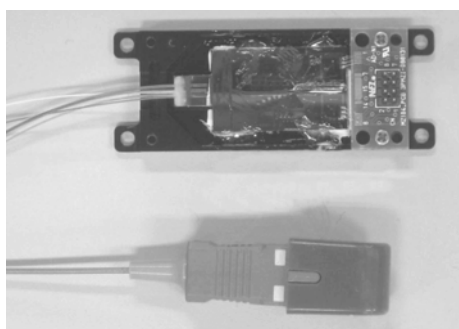


Fig. 10 Image of the DQPSK demodulator module.

grooves are set so that they are symmetrical with respect to the half-wave plate. When they are driven, the thin film heaters generate thermal stress around the core. As we position the heaters so that they are symmetrical with regard to the half-wave plate and drive them simultaneously, the half-wave plate can cancel out the generated stress.

Figure 9 shows the PDF change when electric power is applied to the thin film heaters. When the power is only applied to the heater on one side, we observe a considerable PDF increase. In contrast, when we drive the heaters on both sides simultaneously, there is no degradation in the PDF, as the stress generated at the heaters is canceled out. It should be noted that our proposed interwoven configuration enables us to install all the phase shifters in a symmetrical manner unlike the conventional configuration [9], and allows us to suppress the PDF degradation.

3.2 Fabrication and Evaluation Results

We fabricated athermal DQPSK demodulators with the athermalization methods described in Sect.2 and the interwoven configuration described in the previous section. The refractive index difference and waveguide core thickness were 1.5% and 4.5 μm, respectively. The FSRs of the two DLIs were set at 21.9 GHz. Figure 10 shows the packaged athermal DQPSK demodulator. The package size was

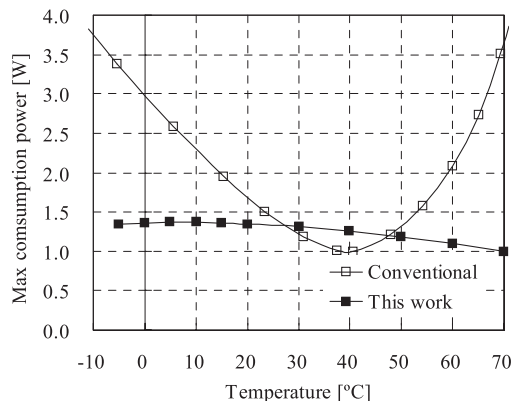


Fig. 11 Maximum power consumption of conventional and athermal demodulator.

40 × 12 × 5.2 mm.

Figure 11 shows the power consumption of our fabricated athermal DQPSK demodulator as a function of ambient temperature. The result for a conventional demodulator with TEC control is also shown for comparison. Both demodulators have a power consumption offset of 1.0 W, which is the maximum power consumption of heaters for tuning the DLI spectrum of both the I and Q channels to the ITU-T grid frequencies. The conventional demodulator requires an additional power consumption of about 2 W to stabilize the chip temperature with the TEC. In contrast, the athermal demodulator can stabilize the chip temperature without consuming any power. The maximum power consumption of the athermal demodulator was only 1.4 W including the power needed to compensate for the residual temperature dependence described in Sect. 2.1, and is 60% lower than that of a conventional demodulator [9].

Figure 12(a) shows the transmission spectra of the demodulator at ambient temperatures of -5, 20 and 70 °C. The residual temperature dependence of the chip was compensated with the heaters. The phase differences between the I and Q DLIs were adjusted to 90° also by using the phase shifters. The transmission spectra at different ambient temperatures are in good agreement. This result shows that the DLI spectrum is successfully athermalized. The measured insertion loss of the demodulator was 5.8 dB.

Figure 12(b) shows our measured maximum PDF within the C-band as a function of ambient temperature. It should be noted that the wavelength dependence of the PDF was less than 30 MHz within the C-band. As shown in the figure, the PDF was better than 170 MHz, and had very little temperature dependence. This result indicates that the birefringence was successfully athermalized.

We measured the bit error rate (BER) with our demodulator by changing the OSNR over a -5 to 70 °C temperature range. Figure 13(a) shows BER vs. OSNR at different temperatures. Figure 13(b) shows the temperature dependence of the OSNR that was required for BER = 10⁻³. The deviation was less than 0.1 dB, and this result shows that the fabricated demodulator exhibited no OSNR temperature de-

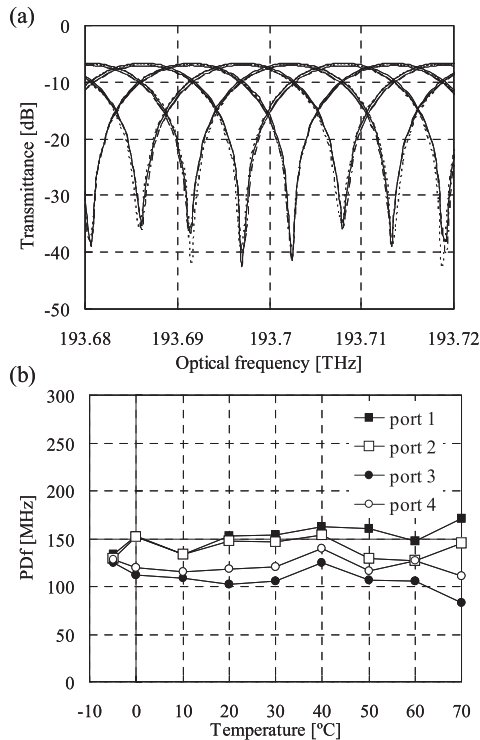


Fig. 12 (a) The transmission spectra of all four demodulator ports at -5°C , 20°C and 70°C are overwritten. (b) Temperature dependence of fabricated demodulator for all port.

pendence. With our conventional DQPSK demodulator with the TEC, the OSNR at $\text{BER} = 10^{-3}$ was 12.45 dB, and this was almost the same as that of our developed demodulator without the TEC.

We also investigated the stability with respect to the temperature change caused by the phase shifter. With the TEC, even if the heat was induced around the phase shifter, the chip temperature could be kept constant. However, without the TEC, the heat from phase shifter on a chip changed the chip temperature itself, and this may interfere with the demodulator performance. This problem may occur when the DLI characteristics are tuned to follow the wavelength deviation of the input DQPSK signals in a real system. So we measured the step response of the BER when the phase shifter switched to the on state.

Figure 14 shows the time evolution of the chip temperature and BER. We preliminarily tuned the center frequency of the DLI to the signal frequency with the heater power, and we adjusted OSNR to make BER became about 10^{-3} by adding ASE noise to the signal. For time = 0, we applied a heater power of 350 mW. After applying the power, the chip temperature gradually increased. On the other hand, the BER became rapidly 10^{-3} within 100 ms and did not change as the temperature increased. This power corresponded to a change of about 15 GHz in the DLI spectrum. In a real system, such a large frequency change or the incidental temperature change owing to the heat from the phase shifter may not occur. Even when there is the rapid temperature change

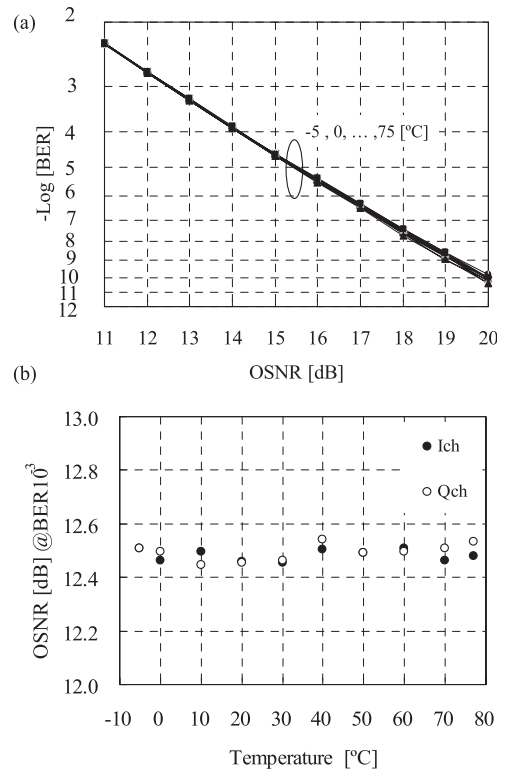


Fig. 13 Bit error rate measurement of our demodulator. (a) OSNR dependence on bit error rate over a -5 to 70°C for channels I and Q. (b) OSNR over a -5 to 70°C temperature range at a bit error rate of 10^{-3} .

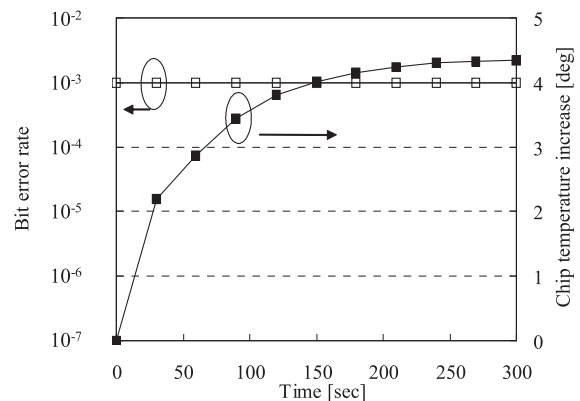


Fig. 14 Change of bit error rate and chip temperature while the phase shifter was on state at time = 0. The power to the phase shifter was 350 mW, which corresponded to a demodulator frequency shift of 15 GHz.

owing to the phase shifter with such a large power, our demodulator continued to provide good performance.

We also investigated the reliability of our chip. As shown in Fig. 15, the Pdf change was less than ± 20 MHz over 5000 hours. This value was almost the same as the accuracy limit of the measurement. From this result, we confirmed that our demodulator had good reliability.

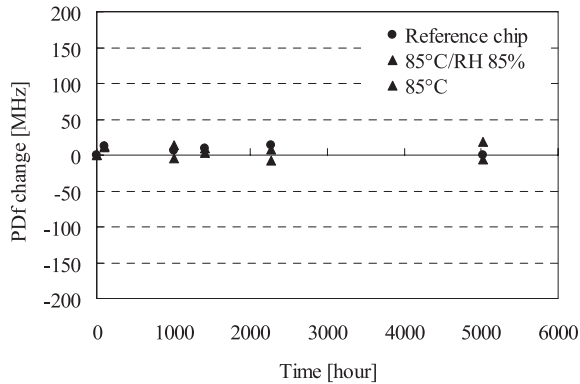


Fig. 15 Reliability test. High temperature and high humidity storage and high temperature storage was done. Reference chip was kept in the room temperature. The test was done with the bare chip.

4. Conclusions

We studied the athermalization of a silica-based DQPSK demodulator. We described two athermalization methods; the athermalization of the transmission spectrum and the athermalization of the polarization property. These methods were successfully demonstrated by reducing the temperature dependence of the refractive index and birefringence of the waveguides. By taking account the loss imbalance due to the resin-filled grooves, we compensated the temperature dependence of the refractive index of the waveguide without degrading the extinction ratio of the DLI. In addition, we tuned the glass expansion to reduce the temperature dependence of the waveguide birefringence, and we achieved an athermal PDF. As a result, the temperature dependence of the DQPSK demodulator was sufficiently low during demodulation, and the TEC became unnecessary. This helped us to reduce the maximum power consumption and the module thickness by 60% and 45%, respectively, compared with the conventional values. We also examined the response and reliability of our demodulator, and we confirmed that our demodulator exhibited stable demodulation performance and long-term reliability.

References

- [1] Y. Sakamaki, et al., "Low power consumption DQPSK demodulator using silica-based planar lightwave circuit," *IEEE Photonics Technol. Lett.*, vol.21, no.14, pp.978–980, 2009.
- [2] K. Hattori, et al., "Low power consumption PLC-type 43 Gb/s DQPSK demodulator," *Proc. OFC 2009*, San Diego, CA, Paper OWO4, 2009.
- [3] T. Kataoka, et al., "Field transmission by using a commercially-ready 43 Gbit/s DWDM system employing RZ-DQPSK transponders in high PMD installed fiber," *OFC2007*, 2007.
- [4] T. Matsuda, et al., "43 Gb/s Pre-chirped RZ DQPSK WDM signal transmission over 500-km and 12 OADM nodes," *ECOC 2006*, pp.1–2, Sept. 2006.
- [5] J.Y.C. Hsieh, et al., "Athermal demodulator for 42.7-Gb/s DPSK signals," *ECOC 2005*, vol.4, p.827, 2005.
- [6] Y.K. Lizý, et al., "Phase-tunable low-loss, S-, C-, and L-band DPSK and DQPSK demodulator," *Photonics Technol. Lett.*, vol.19, no.23, p.1886, 2007.
- [7] H. Takahashi, "Planar lightwave circuit devices for optical communication: Present and future," *Proc. SPIE 5246*, pp.520–531, 2002.
- [8] C.R. Doerr, et al., "Polarization-Insensitive planar lightwave circuit dual-rate Mach-Zehnder delay-interferometer," *Photonics Technol. Lett.*, vol.18, no.16, pp.1708–1710, 2006.
- [9] M. Oguma, et al., "Single DLI-based 1×4 DQPSK demodulator," *ECOC'2007*, vol.4, pp.147–148, 2007.
- [10] M. Okuno, et al., "Birefringence control of silica waveguides on Si and its application to a polarization-beam splitter/switch," *J. Lightwave Technol.*, vol.12, no.4, pp.625–633, 1994.
- [11] I.P. Kaminow, "Polarization in optical fibers," *IEEE J. Quantum Electron.*, vol.QE-17, no.1, pp.15–22, Jan. 1981.
- [12] K. Takada, et al., "Polarization crosstalk dependence on length in silica-based waveguides measured by using optical low coherence interference," *J. Lightwave Technol.*, vol.16, no.8, pp.1413–1422, 1998.
- [13] H. Kawakami, et al., "Analysing the penalty induced by PD of DLI in DQPSK receiver using novel measuring technique," *Electron. Lett.*, vol.43, no.2, p.122, 2007.
- [14] H. Kim, et al., "Robustness to laser frequency offset in direct-detection DPSK and DQPSK systems," *J. Lightwave Technol.*, vol.21, no.9, pp.1887–1891, 2003.
- [15] Y. Nasu, et al., "Reduction of polarization dependence of PLC mach-zehnder interferometer over wide wavelength range," *J. Lightwave Technol.*, vol.27, no.21, pp.4814–4820, 2009.
- [16] Y. Nasu, et al., "Polarization insensitive single-DLI based DQPSK demodulator with asymmetric half-wave plate configuration," *J. Lightwave Technol.*, vol.27, no.23, pp.5348–5355, 2009.
- [17] Y. Nasu, et al., "Birefringence suppression of UV-induced refractive index with grooves in silica-based planar lightwave circuits," *Electron. Lett.*, vol.41, no.20, p.1118, 2005.
- [18] Y. Sakamaki, et al., "Operation range enhancement of silica waveguide 43 Gbit/s DQPSK demodulator by using stress release grooves," *LEOS 2008*, pp.449–450, Nov. 2008.
- [19] Y. Nasu, et al., "Polarization insensitive DLI-based DQPSK demodulator with asymmetric half-wave plate configuration," *OFC2008*, pp.1–3, 2008.
- [20] S. Kamei, et al., "1.5%- Δ athermal arrayed-waveguide grating multi/demultiplexer with very low loss groove design," *IEEE Photonics Technol. Lett.*, vol.17, no.3, pp.588–590, 2005.
- [21] T. Hashimoto, et al., "Compact DQPSK demodulator with interwoven double Mach-Zehnder interferometer using planar lightwave circuit," *Proc. ECOC 2008*, Brussels, Belgium, Paper Mo.3.C.2., 2008.
- [22] B. Huiszoon, et al., "Integrated parallel spectral OCDMA en/decoder," *IEEE Photonics Technol. Lett.*, vol.19, no.7, pp.528–530, 2007.
- [23] A.M. Vengsarkar, et al., "Long-period fiber gratings as band-rejection filters," *J. Lightwave Technol.*, vol.14, no.1, pp.58–65, 1996.
- [24] M.T. Hill, et al., "Optimizing imbalance and loss in 2×2 3-dB multimode interference couplers via access waveguide width," *J. Lightwave Technol.*, vol.21, no.10, pp.2305–2313, 2003.
- [25] A. Kilian, et al., "Birefringence free planar optical waveguide made by flame hydrolysis deposition (FHD) through tailoring of the over-cladding," *J. Lightwave Technol.*, vol.18, no.2, p.193, 2000.



Yusuke Nasu received B.S. and M.S. degrees in electronic engineering from the University of Tokyo in 2000 and 2002, respectively. He joined NTT Photonics Laboratories, Kanagawa, Japan, in 2002, where he has been engaged in research on silica-based planar lightwave circuits (PLCs) for optical communication systems.



Takashi Saida received B.S., M.S., and Ph.D. degrees in electrical engineering from Tokyo University, Tokyo, Japan, in 1993, 1995, and 1998, respectively. In 1998, he joined NTT Corporation, Ibaraki, Japan, where he engaged in the research and development of functional silica-based planar lightwave circuits (PLCs).



Yohei Sakamaki received B.S. and M.S. degrees in material science and engineering from Kyoto University, Kyoto, Japan in 2002 and 2004, respectively. In 2004, he joined, NTT Photonics Laboratories, where he engaged in research on optical waveguide design using the wavefront matching (WFM) method.



Hiroshi Takahashi received B.S. and M.S. degrees in electrical engineering from Tohoku University in 1986 and 1988, respectively. In 1988, he joined NTT Laboratories where he engaged in research on the design and fabrication of silica-based optical waveguide devices. He is currently a research group leader at NTT Photonics Laboratories.



Kuninori Hattori received a B.E. degree in metallurgy from Waseda University, Japan, in 1987, and M.S. and Ph.D. degrees in material science from the Tokyo Institute of Technology in 1989, and 1996, respectively. From 1989, he worked in NTT's Photonics Labs., NTT, Atsugi in 2007.



Yasuyuki Inoue received B.S., M.S., and Ph.D. degrees in electronics engineering from Kyushu University, Fukuoka, in 1987, 1989, and 1998, respectively. He joined Nippon Telegraph and Telephone Corporation (NTT) in 1989. Since then he has been engaged in research on silica-based planar lightwave circuits (PLCs). He is now a senior research engineer in NTT Photonics Laboratories.



Shin Kamei received B.S., M.S. and Ph.D. degrees in physics from the Tokyo Institute of Technology, Japan, in 1996, 1998 and 2008, respectively. He joined NTT Photonics Laboratories, Japan, in 1998, where he engaged in research on silica-based planar lightwave circuits (PLCs). Dr. Kamei is currently with NTT Electronics Corp.



Toshikazu Hashimoto received B.S. and M.S. degrees in physics from Hokkaido University, Japan, in 1991 and 1993, respectively. Since joining NTT Photonics Laboratories in 1993, he has been engaged in research on the hybrid integration of semiconductor lasers and photodiodes on silica based planar lightwave circuits and in theoretical research on the WFM.